Proceedings of the 12th International Conference on
Aluminium Alloys, September 5-9, 2010, Yokohama, Japan

pp. 1559-1566


# Re-examination of Deformation Mechanism Map of Pure Aluminum

Eiichi Sato[1], Yoshimasa Takayama[2], Toshiya Shibayanagi[3] and Koichi Kitazono[4]

[1]Institute of Space and Astronautical Science, Japan Aerospace Exploration Agency, 3-1-1 Yoshinodai, Chuo, Sagamihara 252-5210, Japan

[2]Department of Mechanical Systems Engineering, Utsunomiya University, Utsunomiya 321-8585, Japan

[3]Joining and Welding Research Institute, Osaka University, 11-1 Mihogaoka, Ibaraki 567-0047, Japan

[4]Graduate School of System Design, Tokyo Metropolitan University, 6-6 Asahigaoka, Hino 191-0065, Japan

Deformation behavior of pure aluminum was re-examined, particulary addressing low-temperature creep, high-speed deformation, dynamic recrystallization, and friction stir regions using three grades of pure aluminum (5N, 4N and 2N). The deformation mechanism map of pure aluminum was, then, modified: (1) a new low-temperature region with low activation energy was added, and (2) the dynamic recrystallization region was extended towards 0.32 $T_m$ ($T_m$: the melting point).

***Keywords:*** *pure aluminum, deformation mechanism map, low temperature, high speed deformation, dynamic recrystallization, friction stir*

## 1. Introduction

Deformation mechanisms of metals are arranged in an Ashby-type deformation mechanism map [1]. The map is composed by normalized stress $\sigma/G$, homologous temperature $T/T_m$ and strain rate; if two of these parameters are given, then the working deformation mechanism is determined. Langdon et al. modified the map using an axis of the normalized grain size $d/b$ [2] or the reciprocal of the homologous temperature: $T_m/T$ [3]. However, recent progress in the study of low-temperature or high-speed (friction stir or impact) deformation requires extension of the map towards both low strain-rate and high strain-rate sides.

This study was undertaken to re-examine and re-draw the deformation mechanism map of pure Al. Wespecifically examined the low-temperature and low-strain rate region (§2), high-speed deformation region at room temperature (§3), intermediate-strain rate and temperature region where dynamic recrystallization takes place (§4), and high-speed and high-temperature region by friction stirring (§5). Finally, a revised deformation mechanism map was created.

The materials we used were high-purity Al of 5N (5N-Al), high-purity Al of 4N (4N-Al) and commercial pure Al of A1050 (2N-Al). Plates of 5N-Al with 1 mm thickness were prepared by hot rolling followed by annealing, providing an equiaxial grain structure with grain size of about 140 μm. Cubic specimens of 10×10×10 mm$^3$ were also prepared.

## 2. Low-temperature region

### 2.1 Purpose

In the deformation mechanism map of pure Al produced by Frost and Ashby [1], creep deformation is expected to proceed even at temperatures less than 0.4 $T_m$. However, because of the lack of experimental data, the low-temperature region has not been examined well. On the other hand, creep behavior at ambient temperature was observed in h.c.p. metals [4]. Therefore, this section presents a re-examination of the low-temperature creep region using high-purity Al.

### 2.2 Experimental

Creep tests were performed at temperatures of 253–523 K on the samples of 5N-Al, 4N-Al and 2N-Al with average grain sizes of 140, 100 and 50 μm, respectively, with the loading direction parallel to the rolling direction. Optical microscopy was conducted before and after the creep test on the surface, which was polished mechanically using colloidal silica before the creep test.

**2.3 Results**

All specimens showed significant creep behavior even below room temperature. The 5N-Al shows a stress exponent of about 5.0 below 373 K (0.4 $T_m$), and 4.0 above 473 K. In addition, 4N-Al shows similar behavior; 2N-Al shows slightly larger stress exponent than the others.

Figure 1 shows an Arrhenius plot of the three specimens at $\sigma/E = 3.0 \times 10^{-4}$. This plot shows two regions with different apparent activation energies, whose border is about 420 K. Both 5N-Al and 2N-Al show apparent activation energy of 75 kJ/mol above this temperature. All samples show 20–30 kJ/mol at the lower temperatures.

Figure 2 shows the double logarithmic plot of creep tests with several grain sizes; all data points locate on a single line. It is clearly concluded that the creep rate is independent of the grain size. In addition, this creep phenomenon occurs above the 0.2% proof stress $\sigma_{0.2}$, which means that the strain hardening has already proceeded before the creep starts.

**2.4 Discussion**

Luthy et al. [5] and Ishikawa et al. [6], in addition to the present authors investigated the creep behavior in the low-temperature region. Below 420 K, the Arrhenius plot of the three studies branches into two lines; one line is reported by Luthy with 80 kJ/mol, which is close to the pipe-diffusion activation energy of Al. On the other hand, Ishikawa reported 20 kJ/mol below 420 K, which agrees well with data obtained in the present study.

Figure 3 depicts selected creep data of Luthy, Ishikawa and the authors. Luthy et al. estimated the activation energy using data in the power-law breakdown region. Because the effect of temperature dependency of shear modulus is significant in the power-law breakdown region [1], they might overestimate the activation energy. On the other hand, Ishikawa and we respectively obtained the creep behavior near and in the power-law region. Therefore, the activation energy of low-temperature creep of pure Al is inferred as 30 kJ/mol.

For pure Al below 420 K, the stress exponent is 4–5 and the activation energy is 20–30 kJ/mol, which implies that dislocations contribute to the creep deformation but that the diffusion does not. The ambient temperature creep of h.c.p. metals is one such type of creep [7]. The creep occurs at less than 0.2% proof stress; only the single slip system

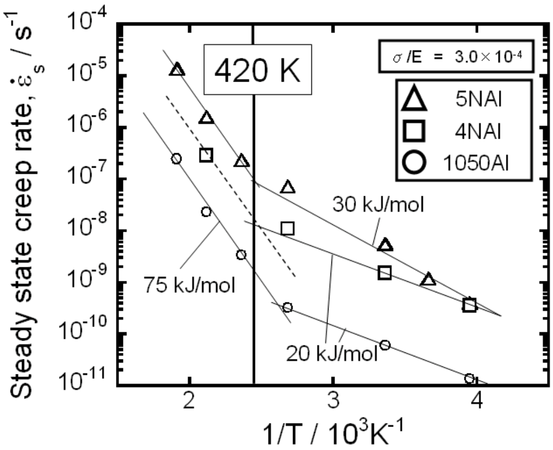


**Fig. 1** Arrhenius plot for three pure Al.

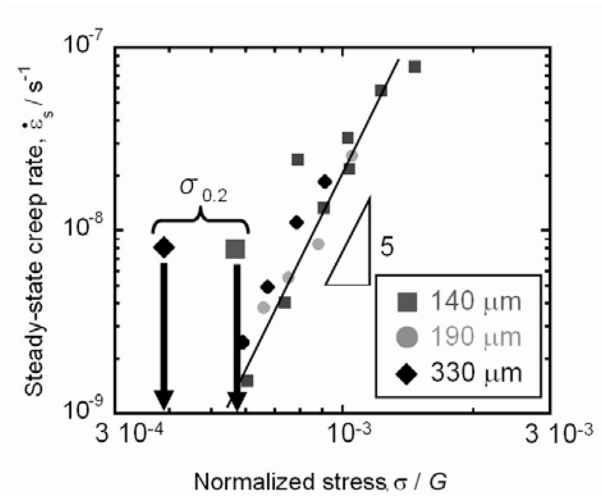


**Fig. 2** Grain size dependency of the creep behavior for 5N-Al sample crept at 300 K

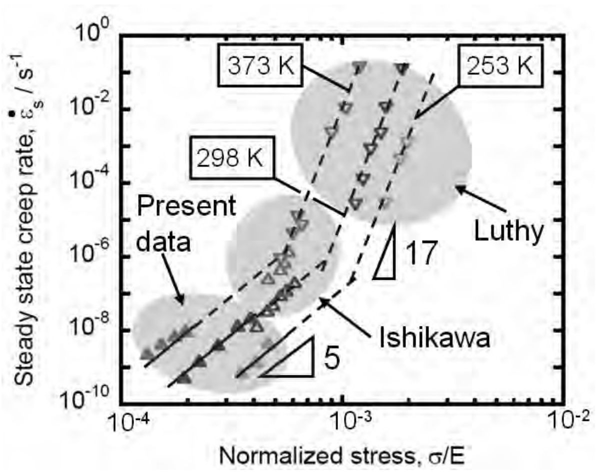


**Fig. 3** Double logarithmic plots of selected creep data of Luthy, Ishikawa and the authors in the low-temperature region of 5N-Al.

acts. Dislocations pile up on the grain boundary without a dislocation intersection, and are absorbed into grain boundaries resulting in continuing creep deformation with grain boundary sliding. In the case of pure Al, creep occurs above the 0.2% proof stress; the secondary slip system also acts. In addition, the creep behavior is independent of the grain size. Therefore, the results suggests that low-temperature creep of pure Al is a different deformation mechanism from the ambient temperature creep of h.c.p. metals.

### 2.5 Summary

Low-temperature creep behavior of pure Al was investigated. An extremely low-activation energy region was obtained, which has not been reported in the Ashby's map. The low-temperature creep region has the following features.

(1) The stress exponent is about 4–5; the creep deformation is independent of the grain size.
(2) Creep occurs at above 0.2% proof stress.
(3) The secondary slip system acts, and slip lines propagate to the adjacent grain.

## 3. High speed deformation region

### 3.1 Purpose

High-speed deformation of several Al alloys has been reported by Higashi et al. [8] by which flow stress and the strain rate dependency increase rapidly as the strain rate increases above $10^3$ $s^{-1}$. However, a basic study using pure Al without strengthening effects has scarcely been reported, and specimens for high-speed deformation are usually considerably smaller than those for conventional quasi-static deformation. The aim of this section was to examine the high-speed deformation of pure Al using the same specimens as those used for low-speed tests. The load was applied using a hydraulic impact tensile testing machine.

### 3.2 Experimental

Tensile tests were performed at room temperature at strain rates between $10^{-4}$ and $10^{-2}$ $s^{-1}$ using AUTOGRAPH (Shimadzu Co.), and for higher strain rates using DYNAMIC SERVO (Saginomiya Seisakusho Inc.). Specimens were No. 5 specimen of JIS Z2201 with 10 mm gage length, 25 mm gage width and 1 mm thickness for the three pure Al.

### 3.3 Results and discussion

Tensile strengths and 0.2% proof stresses of the three specimens are shown against the strain rate in Fig. 4. The tensile strength decreased concomitantly with increasing the purity of the specimens both in high-speed and low-speed tensile tests. The proof stress also decreased concomitantly with increasing purity up to 4N-Al and saturated between 4N-Al and 5N-Al. In the stress–strain curves, stress oscillation was observed in high-speed tests because of overlapping of the reflected stress at the load cell. Tensile strengths and proof stresses increased with increasing strain rate greater than 10 $s^{-1}$.

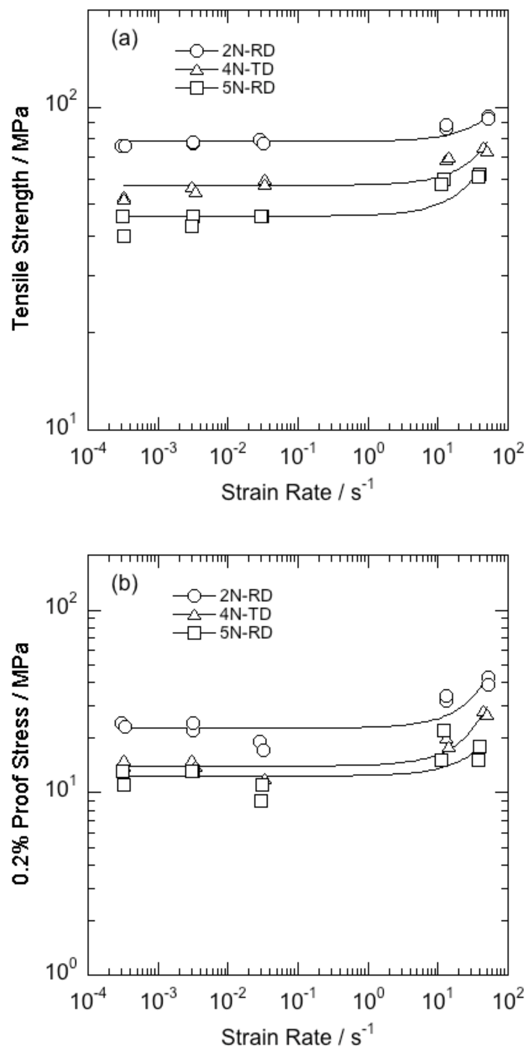


**Fig. 4** Strain rate dependences of tensile strength (a) and 0.2% proof stress (b) in tension of pure Al.

Fracture strains of the three specimens are shown against the strain rate in Fig. 5. In the low-strain rate region, the fracture strain was almost constant at 35% for the three specimens. On the other hand, in the high- strain rate region, fracture strain of 2N-Al increased to 40%, whereas those of 4N-Al and 5N-Al remain constant.

The main impurities in pure Al are Fe and Si. In 4N-Al and 5N-Al, the impurities are dissolved in Al, while in 2N-Al, some of them precipitate as $Al_3Fe$ and Si, engendering higher proof stress of 2N-Al than 4N-Al and 5N-Al.

### 3.4 Summary

Tensile tests from low speed to high speed were executed to obtain the following results:

(1) The tensile strength and the 0.2% proof stress were constant at less than $10^{-1}$ $s^{-1}$ but increased at greater than $10^{-1}$ $s^{-1}$.

(2) The tensile strength decreased concomitantly with increasing purity; the proof stress also decreased but saturated between 4N-Al and 5N-Al.

(3) The fracture strain was almost constant in the low strain rate region. In the high strain rate region, it increased for 2N-Al but remained constant for 4N-Al and 5N-Al.

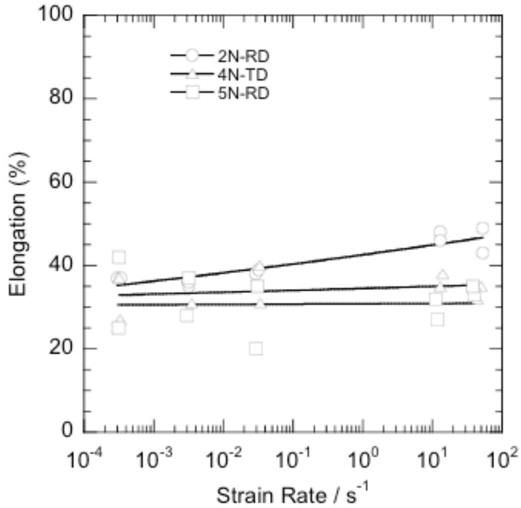


**Fig. 5** Strain rate dependence of fracture strain of pure Al.

## 4. Dynamic recrystallization region

### 4.1 Purpose

Recrystallization involves the formation of new strain-free grains in certain parts of the sample and the subsequent growth of these to consume the deformed or recovered microstructure [9]. It is convenient to divide recrystallization into two regions, "nucleation", which corresponds to the first appearance of new grains and "growth", during which the new grains replace deformed materials. It is well known that various factors affect the rate of recrystallization: (i) the deformed structure, (ii) the grain orientations, (iii) the original grain size, (iv) solutes, (v) the deformation temperature and strain rate, and (vi) the annealing condition. Two important factors to elucidate microstructural control are the amount of strain and the solutes.

This section reveals the onset condition of discontinuous dynamic recrystallization (DDRX) in pure Al in the deformation mechanism map. The static or dynamic restoration process at room temperature after the same temperature deformation was observed sequentially using in-situ scanning electron microscopy with electron backscattered diffraction pattern (SEM/EBSD) analysis.

### 4.2 Experimental

Specimens were 5N-Al plate with 1-mm thickness and 10-mm cubes of 5N-Al, 4N-Al and 2N-Al. Each specimen was compressed at room temperature (298 K; $0.32T_m$) with crosshead speed of $1.7 \times 10^{-5}$ $s^{-1}m$ up to 50% compression. After compression, the specimens were polished and EBSD analysis was performed after several intervals. The identical region was analyzed with area of $500 \times 500$ $\mu m^2$ in each specimen. In addition, the Vickers hardness change at room temperature was measured after 51.9% compression.

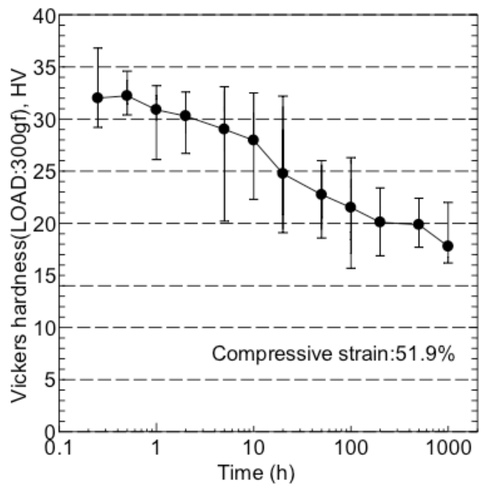


**Fig. 6** Hardness change at room temperature after compression test of 5N-Al.

### 4.3 Hardness change at room temperature

Figure 6 shows the hardness change of 5N-Al after compression of 52%. Hardness decreased from 32.0HV to 21.5HV, which implies that the static restoration (recovery or recrystallization) took place at room temperature.

### 4.4 Compression behavior at room temperature

Figure 7 shows the load–displacement curve of compression of a cube specimen for ND direction with lubricant. It shows no stress oscillation attributable to DDRX.

### 4.5 Structural development at room temperature

Figure 8(a) shows an Inverse Pole Figure (IPF) Map of 5N-Al after 2 hours at room temperature after compression of 50%; Fig. 8(b) shows that after 10 hours. In the surrounding area of Fig. 8(a), a group of small grains with strains inside are observed. During compression, recrystallized grains that are free of strain were probably created. Then they were deformed during the subsequent compression, which implies the occurrence of DDRX during compression at room temperature.

After Fig. 8(a), holding at room temperature for 10 hours produced several new grains that are free of strain as presented in Fig. 8(b). These grains grew during subsequent holding for 100 and 1000 hours, which reveals that static recrystallization took place.

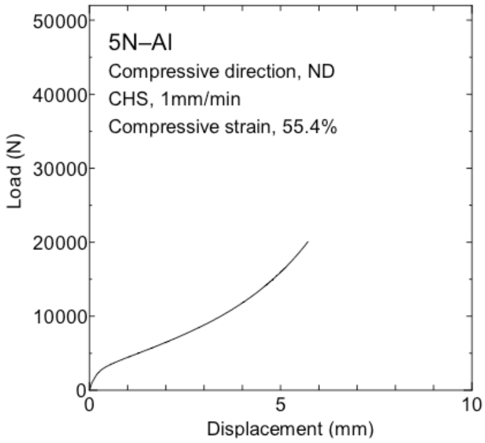


**Fig. 7** Load-displacement curve of compression of the cube specimen for ND direction with lubricant.

### 4.6 Dynamic recrystallization region in the deformation mechanism map

Aluminum having high stacking fault energy has been considered to show dynamic recovery, for that reason, the DDRX region was depicted in shadow with a comment of "scarcely observed" [1]. Nevertheless recent studies by Yamagata [10] and others [11] concluded that in 5N-Al DDRX takes place in a temperature region of 0.44–0.70$T_m$.

The present study revealed that DDRX takes place in the wide temperature region greater than 0.32 $T_m$. Because the occurrence of DDRX is restricted by the Zener-Hollomon parameter, Z, which is a function of stress, the DDRX region in deformation mechanism map is restricted by two parallel lines around stress of $10^{-3}$ $G$. Therefore, we can draw the DDRX region as a rectangle surrounded by the four lines of $T/T_m$ =0.32, $T/T_m$ =1.0, $\tau/G$ =4 × $10^{-4}$ and $\tau/G$ =4 × $10^{-5}\tau/G$, as presented in Fig. 14(b).

### 4.7 Summary

Hardness and EBSD analyses were performed sequentially after compression of 5N-Al at room temperature to obtain the following results:

(1) Hardness apparently decreased implying the occurrence of static restoration at room temperature.

(2) EBSD analyses implied discontinuous recrystallization during compression; that is, DDRX.

(3) Static recrystallization took place during holding at room temperature after compression of 50%.

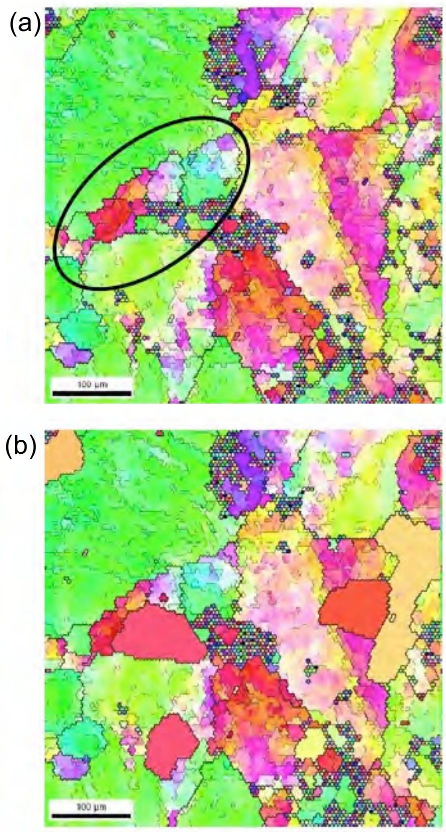


**Fig. 8** IPF Maps of the specimens held at room temperature for 2 and 10 hours after compression test of 5N-Al ((a) and (b), respectively).

## 5. Friction stir region

### 5.1 Purpose

Although friction stir welding (FSW) was originally developed for joining Al alloys, it is now being applied during the fabrication of a wide range of materials [12]. The aim of this section is to study the deformation mode, stress and strain rate, and to understand the characteristic of deformation behavior of the friction stir region. In contrast to complicated flow during FSW, friction stir spot welding (FSSW), being simpler than seam welding, was examined in this study.

### 5.2 Experimental

Specimens were 5N-Al plates and single crystals grown from 4N-Al using a Bridgeman-type furnace. FSSW was performed using facilities produced either by Friction Stir Link or by Hitachi Engineering. The welding tool had a 10-mm-diameter shoulder and a threaded pin with the M4 profile having three flat faces machined, ; it was made of SKD61. The axial load and the torque output during FSSW were measured using a JR3 six-axis load cell. The thermal cycle during FSSW was measured by embedding thermocouples at the tip of the pin and at the outer periphery of the tool shoulder. Spot welded specimens were then supplied for optical microscopy and SEM/EBSD analysis.

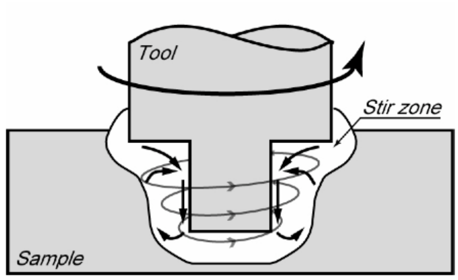


**Fig. 9** Schematic diagram showing formation of a helical vertical rotational flow within SZ.

### 5.3 Results and discussion

Figure 9 represents a schematic diagram showing formation of a helical vertical rotational flow within the stir zone (SZ) formed adjacent to the periphery of the rotating pin [13]. This model suggests that the adjacent region to SZ is subjected to compressive stress by dwelling of SZ, in addition to shear stress by rotating SZ.

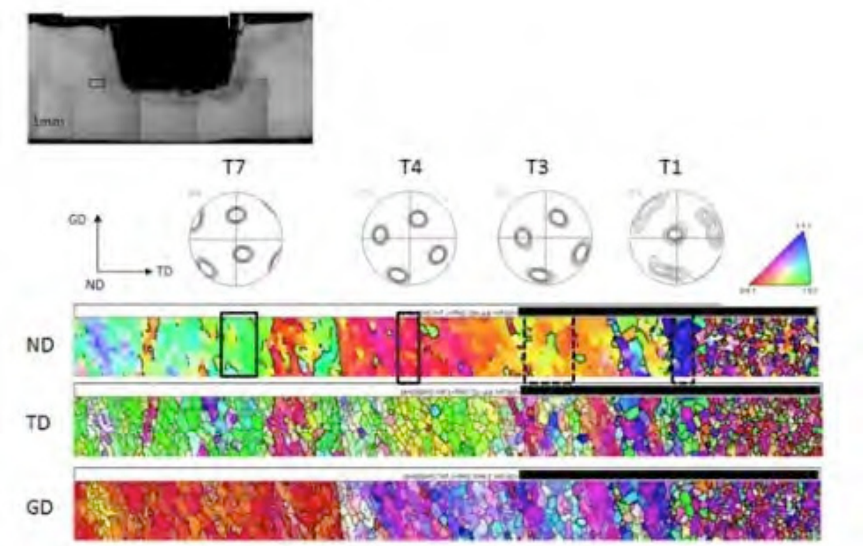


**Fig. 10** Crystal orientation map of SZ.

Figure 10 portrays three orientation maps of SZ after FSSW at 1500 RPM for 2 s on a single-crystal Al specimen of <111>//ND and <110>//TD. The crystal orientation analysis of outside of SZ revealed that the {110} oriented region, which is represented by green color, appeared outside of SZ, as shown in the TD map, which suggests that

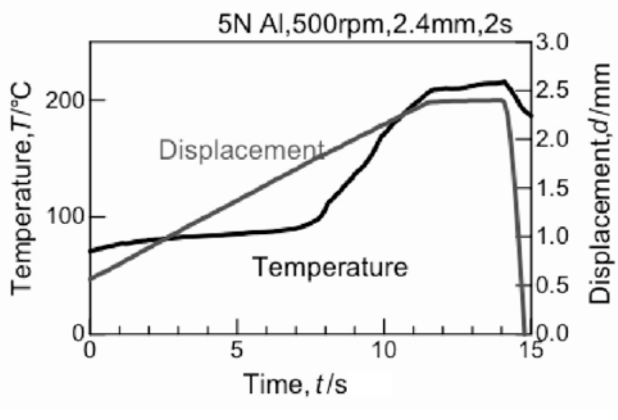


**Fig. 11** Temperature change at the top of the probe in FSSW.

both compressive and shear modes are mutually competing during FSSW.

An example of the measured temperature cycle of FSSW of single-crystal Al is presented in Fig. 11. The temperature increased rapidly during the tool penetration stage and reached 210°C within 11 s. It increased continuously during the 2-s-dwell period. Consequently, the microstructure was formed in the temperature range of static or dynamic recrystallization. The highest temperature during FSSW of 5N-Al was shown against rotation speed in Fig. 12, which shows a positive dependency.

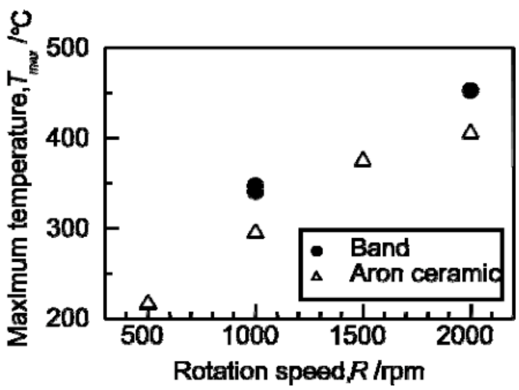


**Fig. 12** Relation between highest temperature and rotation speed during FSSW of 5N-Al.

Figure 13 shows the axial load and torque, which were the measurable mechanical parameters in the present apparatu. The load during the dwell period of 500 RPM being 2.0 kN, the compressive stress was estimated between 22 MPa and 155 MPa ($8.6 \times 10^{-4}$ $G$ and $6.1 \times 10^{-3}$ $G$). The stress of 1000 RPM was also estimated as ranging from $3.5 \times 10^{-4}$ $G$ to $2.4 \times 10^{-3}$ $G$.

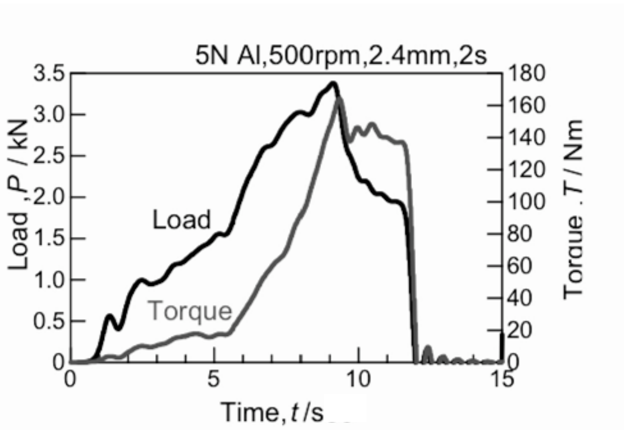


**Fig. 13** Load and torque curves during FSSW of 5N-Al.

The strain rate during FSSW was estimated based on the grain size dependency on Zener-Hollomon parameter during dynamic recrystallization. On FSSW at a rotation speed of 500 RPM, the maximum temperature was 562 K and the resulting grain size was 1.5 μm. Using these parameters, the strain rate was estimated as 1.4 $s^{-1}$ for FSSW of 500 RPM.

### 5.4 Deformation mechanism map

The FSSW region estimated above was temperature of 0.6 $T_m$ and stress between $8.6 \times 10^{-4}$ $G$ and $6.1 \times 10^{-3}$ $G$, and 0.75 $T_m$ and $3.5 \times 10^{-4}$ $G$ and $2.4 \times 10^{-3}$ $G$, which can be shown in the deformation mechanism map. However since several deformation modes are acting during FSSW, the FSSW region requires further investimation.

### 5.5 Summary

Using single-crystal specimens, the existence of compressive stress was established, and using polycrystalline specimens, temperature measurement, stress estimation and strain rate estimation during the FSSW process were demonstrated. Using these parameters, complicated flow conditions during FSSW were depicted in the deformation mechanism map.

## 6. Conclusions

The deformation mechanism map of pure Al was re-examined, particularly addressing low-temperature creep, high-speed deformation, dynamic recrystallization and friction stir regions using three grades of pure aluminum (5N, 4N and 2N). The following results were obtained:

(1) Low-temperature region: a new region with an activation energy of 20 kJ/mol and a stress exponent of four was found and was depicted in the map.

(2) High-speed deformation region: the strength remains constant up to $10^{-1}$ $s^{-1}$; it then increases with further increase in the strain rate.

(3) Dynamic recrystallization region: discontinuous dynamic recrystallization (DDRX) occurs commonly at temperatures greater than 0.32 $T_m$ with stresses around $\tau/G=10^{-3}$ in high-purity aluminum.

(4) Friction-stir region: temperature, stress and strain rate during FSSW have been estimated. Consequently, the map position has been identified.

Finally, the deformation mechanism map of Al was modified from Fig. 14(a) to Fig. 14(b) by addition of the new low-temperature creep region and the dynamic recrystallization region, which was extended towards 0.32 $T_m$.

(a)

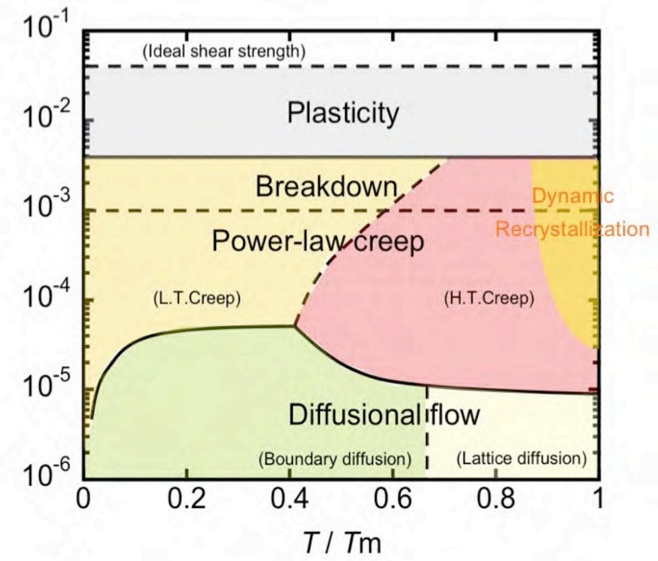


(b)

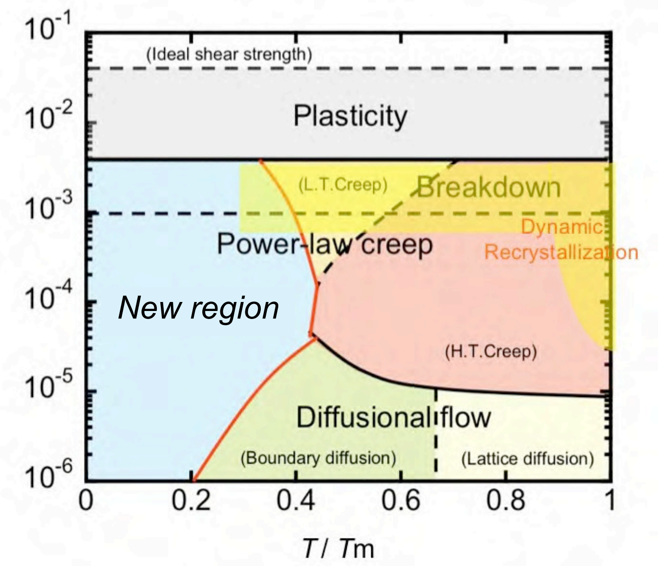


**Fig. 14** (a) Original deformation mechanism map of pure Al by Ashby, and (b) revised version by the present authors.

**Acknowledgements**

This research was supported by The Light Metal Educational Foundation Inc. as Integrated Advanced Research. The pure Al used in this study was offered by Sumitomo Light Metal Industries. The authors express their sincere thanks to them.

## References

[1] H. J. Frost, M. F. Ashby: *Deformation mechanism maps* (Oxford Pergamon Press, 1982).
[2] F.A.Mohamed and T.G.Langdon: Metall. Trans., 5 (1974) 2339–2345.
[3] T.G.Langdon and F.A.Mohamed: J. Mater. Sci., 13 (1978) 473–482.
[4] H. Tanaka, T. Yamada, E. Sato, I. Jimbo: Scripta Mater. 54 (2006) 121–124.
[5] H. Luthy, A. K. Miller, O. D. Sherby: Acta. Metal 28 (1980) 169–178.
[6] K. Ishikawa, M. Maehara, Y. Kobayashi: Mater. Sci. Eng., A322 (2002) 153–158.
[7] T. Matsunaga, T. Kameyama, K. Takahashi, E. Sato: Mater. Trans. 50 (2009) 2865–2872.
[8] K. Higashi, T. Mukai, K. Umezu, S. Tsuchida, S. Tanimura: J. Society of Materials Science, Japan, 39 (1990) 1619–1624, in Japanese.
[9] J.F. Humphreys, M. Hatherly: *Recrystallization and Related Annealing Phenomena*, 2nd Ed. (Elsevier Science, 2004) pp.215–267.
[10] H. Yamagata: Acta Metall. Mater., 43 (1995) 723–732.
[11] D. Ponge, M. Bredehoft and G. Gottstein: Scripta Mater., 37 (1997) 1769–1775.
[12] R. Mishra and Z. Y. Ma: Mater. Sci. Eng., R50 (2005) 1–78.
[13] P. Su, A. Gerlich, T. H. North, G. J. Bendzak: Metall. Mater. Trans., 38A (2007) 584–595.